Geomechanics and Engineering, *Vol. 30, No. 2 (2022) 201-210*
https://doi.org/10.12989/gae.2022.30.2.201

The characteristics of subgrade mud pumping under various water level conditions

Yu Ding[1], Yu Jia*[1], Xuan Wang[1,2], Jiasheng Zhang[1,2], Hao Luo[1], Yu Zhang[1] and Xiaobin Chen[1,2]

[1]*Geotechnical Engineering, School of Civil Engineering, Central South University, 22 South Shaoshan Road, Changsha, Hunan 410083, China*
[2]*National Engineering Research Center of High-Speed Railway Construction Technology, Central South University, 22 South Shaoshan Road, Changsha, Hunan 410083, China*

(Received January 4, 2021, Revised June 8, 2022, Accepted June 26, 2022)

Abstract. This paper presents a study regarding the influence of various water levels on the characteristics of subgrade mud pumping through a self-developed test instrument. The characteristics of mud pumping are primarily reflected by axial strain, excess pore water pressure, and fine particle migration. The results show that the axial strain increases nonlinearly with an increase in cycles number; however, the increasing rate gradually decreases, thus, an empirical model for calculating the axial strain of the samples is presented. The excess pore water pressure increases rapidly first and then decreases slowly with an increase in cycles number. Furthermore, the dynamic stress within the soil first rapidly decreases and then eventually slows. The results indicate that the axial strain, excess pore water pressure, and the height and weight of the migrated fine particles decrease significantly with a low water level. In this study, when the water level is 50 mm lower than the subgrade soil surface, the issue of subgrade mud pumping no longer exist.

Keywords: axial strain; excess pore water pressure; fine particle migration; heavy-haul railway; subgrade mud pumping; water levels

1. Introduction

Heavy-haul railway transportation has become one of the leading freight modes in many countries, such as China, Australia, Canada, and the United States (Singh *et al*. 2019, Leng *et al*. 2018a, Kashani *et al*. 2017). Compared to an ordinary train, the axle load of a heavy-haul train is larger, and the dynamic stress imposed on the track is more significant. Therefore, heavy-haul railway subgrade issues such as mud pumping are more severe (Yang *et al*. 2021, Bian *et al*. 2016, Indraratna *et al*. 2017, Tang *et al*. 2018). The mud from the subgrade pollutes the ballast, reducing its drainage and bearing capacity; thus, severely threatening the safety of the train's operation (Indraratna *et al*. 2018, Hussaini *et al*. 2016, Indraratna *et al*. 2011, Trani and Indraratna 2010a, b, Saride *et al*. 2013).

Water is one of the key factors in determining whether subgrade mud pumping or not (Duong *et al*. 2014, Liu *et al*. 2013, Indraratna *et al*. 2020a, b). When the subgrade is inadequately drained or in a saturated state, it accelerates the mud pumping process. Therefore, improving the drainage capacity of the subgrade can effectively inhibit the occurrence of subgrade mud pumping. Indraratna *et al* (2010, 2009, 1998) studied the characteristics of deformation and excess pore water pressure in clay samples with and without a prefabricated vertical drain (PVD) under cyclic loading. The results showed that PVD effectively prevents the excessive buildup of pore water pressure during cyclic loading, therefore accelerating its dissipation and reducing the axial deformation of the samples. Ito (1984) used horizontal drainage pipes to drain the water inside subgrades in order to mitigate the problems of mud pumping. Li *et al.* (2018) proposed a new type of drainage pressure-relief system for railway tunnel bottoms consisting of a transverse catchment, longitudinal water conduction, and bottom-to-top water drainage system. He then verified that the proposed drainage system effectively drained water and reduced water pressure at the tunnel's bottom. Hasnayn *et al*. (2020, 2017) studied the hydraulic and mechanical properties of railway subgrades with repeated flooding and concluded that sand blanketing on a saturated subgrade was not an effective solution to all subgrade problems. Yu (2013) proposed a composite method of well point dewatering and grouting in order to treat the mud pumping of heavy-haul railway tunnel. The effectiveness of this method was verified via field tests. Qiao (2006) proposed a treatment scheme of setting horizontal and vertical underground blind ditches to drain groundwater in subgrade mud pumping site of the K245 ~ K462 sections in the Jingtong rail line. Yang and Zha (2006) proposed a method of setting horizontal water collecting pipes used to drain the water within the Dabashan tunnel.

Although there are many subgrade drainage methods, relatively few studies focus on the influence of various water levels on the characteristics of subgrade mud pumping. In this study, a self-developed mud pumping test instrument was used to study and analyze the characteristics

*Corresponding author, Mr.
E-mail: jia_yu@csu.edu.cn

ISSN: 2005-307X (Print), 2092-6219 (Online)

Table 1 Physical and mechanical parameters of the clay

Materials	G_s	ω_L / %	ω_P / %	I_P	ρ_{dmax} / (g/cm^3)	ω_{opt} / %	c/ kPa	φ / °
Clay	2.64	33.42	16.64	16.78	1.81	14.7	27.25	24.08
Crushed gravel	2.69	/	/	/	2.08	/	/	/

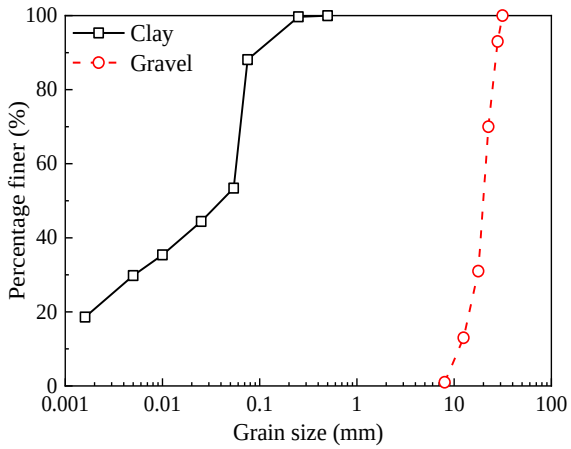

Fig. 1 PSDs of clay and gravel

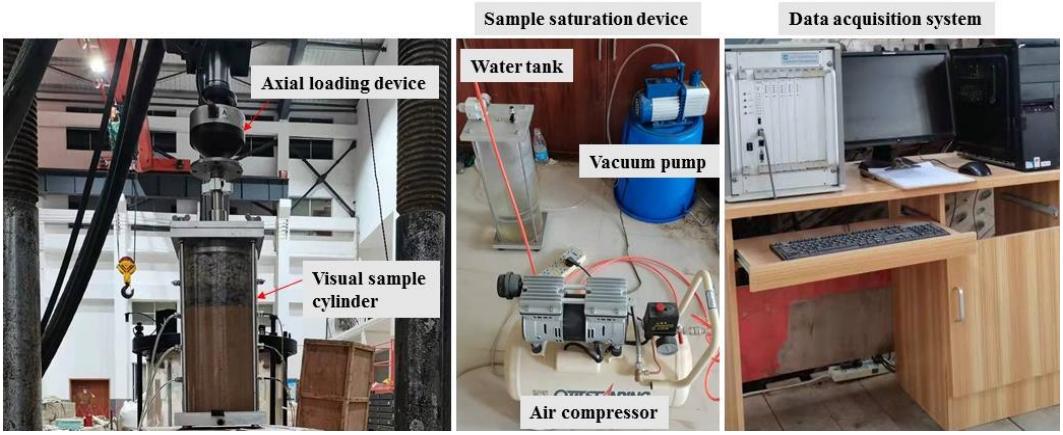

Fig. 2 Test instrument

of subgrade mud pumping under various water levels as well as the characteristics of axial strain, excess pore water pressure, and fine particle migration.

2. Materials and testing methods

2.1 Materials

This study used clay as the subgrade soil, and its basic physical parameters such as specific gravity G_s, Atterberg limits (liquid limit ω_L and plastic limit ω_P), maximum dry density ρ_{dmax}, and optimum moisture content ω_{opt}, were determined and shown in Table 1, furthermore, the clay can be classified as a lean clay. Fig. 1 shows the particle size distribution (PSD) of the clay, the content of the powdered particles (particle size of 0.005-0.075 mm) is 58.3%, and that of the clay particles (particle size of no more than 0.005 mm) is 29.8%. The plastic index and particle size distribution of the clay meet the requirements of soil prone to mud pumping (Nie *et al*. 2018, Leng *et al*. 2018b, Nguyen *et al*. 2019, Chen *et al*. 2019, Nagrale and Patil 2017).

Crushed gravel is used as the ballast filler layer, with a specific gravity of 2.69 and a maximum dry density of 2.08 g/cm^3. The PSD of the gravel is shown in Fig. 1.

2.2 Test model and methods

2.2.1 Test instrument

Fig. 2 shows the self-developed mud pumping test instrument. The test instrument consists of four parts: the axial loading device, transparent sample container, sample saturation device, and the data acquisition system. Three pore

Table 2 Testing programs

Test no.	Water levels / mm	Initial dry density ρ_d / (g/cm^3)	Dynamic stress amplitude σ_d / kPa	Frequency f/ Hz
M-1	+10	1.40	50	5
M-2	+10	1.40	100	1
M-3	+10	1.40	100	5
M-4	+10	1.40	100	10
M-5	+10	1.40	200	5
M-6	0	1.40	100	5
M-7	-10	1.40	100	5
M-8	-50	1.40	100	5
M-9	-150	1.40	100	5

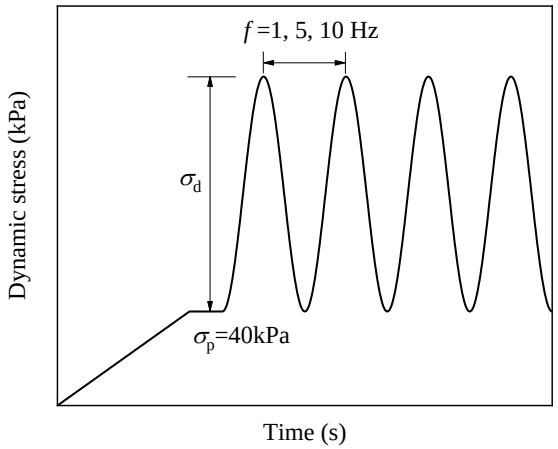

Fig. 3 Loading oscillogram

water pressure sensors (a force sensor with a resistance strain gauge) and three earth pressure sensors (strain type) are installed inside the sample cylinder. The heights of the sensors from the bottom of the sample are 240 mm, 160 mm, and 80 mm (sensors at these three points are represented by A, B, and C, respectively). This instrument can carry out the mud pumping test of saturated soil under cyclic loading, observe the mud pumping situation, and record the axial displacement and axial force of the sample as well as excess pore water pressure and dynamic earth pressure during the test.

2.2.2 Test programs

In this study, we select a sinusoidal wave to simulate a train load. Before applying the cyclic loading, an axial static load of 40 kPa ($\sigma_p = 40$kPa) is applied to simulate the influence of the track load (Bian *et al*. 2016). The cyclic loading amplitude is calculated by Eq. (1) (Bian *et al*. 2016).

$$\sigma_{d\max} = \frac{0.4P_s(1+\alpha v)}{l \times b} \tag{1}$$

Where, $\sigma_{d\max}$ is the maximum dynamic stress on the ballast layer exerted by the train load; P_s is the train axle load; α is the dynamic impact coefficient, which is normally 0.005; v is the running train speed; l and b are the length and width of the sleeper, respectively. For heavy-haul railways, the length and width of the sleeper are generally 2.5 m and 0.25 m. According to Eq. (1), the maximum dynamic stress on the ballast layer exerted by a train with an axial load of 27 tons and a running speed of 80 km/h is about 240 kPa. Therefore, the cyclic loading amplitudes selected in this paper are 50 kPa, 100 kPa, and 200 kPa.

The loading frequency is calculated according to Eq. (2) (Sun *et al*. 2016).

$$f = \frac{v}{L} \tag{2}$$

Where, f is loading frequency, and L is the wheelbase of the train. According to Eq. (2), the frequency corresponding to the train's running speed of 0~100 km/h is 0~14 Hz. In this study, 1 Hz, 5 Hz, and 10 Hz are selected as the representative frequencies. The loading oscillogram is shown in Fig. 3.

The initial dry density of the subgrade soil is controlled at 1.40 g/cm^3. Usually, the buried depth of the subgrade is relatively shallow, and the confining pressure is relatively

Table 3 Parameters of the empirical model (3)

Test No.	Water levels / mm	a	b	R^2
M-1	+10	3.162	0.125	0.95
M-2	+10	4.159	0.188	0.78
M-3	+10	3.543	0.199	0.87
M-4	+10	2.384	0.949	0.75
M-5	+10	5.755	0.214	0.86
M-6	0	2.638	0.630	0.92
M-7	-10	2.074	0.929	0.95
M-8	-50	1.689	0.889	0.87
M-9	-150	0.320	0.461	0.92

small, so we do not consider the influence of the confining pressure in this study.

According to Ding *et al.* (2022), the mud pumping mainly occurs in the upper part of subgrade soil (subgrade soil with a height of 250 mm in this paper), the water levels we selected are +10 mm, 0 mm, -10 mm, -50 mm, and -150 mm, respectively (the subgrade soil surface is selected as the reference surface. If the water level is positive, it means that the water surface is higher than the soil surface; if the water level is negative, it means that the water surface is lower than the soil surface).

The criterion for the end of the test is that the number of cyclic loads reaches 50,000 cycles or the axial strain of the sample reaches 5%. The specific testing program is listed in Table 2.

2.2.3 Sample preparation

The sample size is 178 mm (diameter) × 380 mm (height). The lower part of the sample is filled with clay (subgrade soil) with a height of 250 mm, and the upper part is filled with gravel (ballast) with a height of 130 mm.

The clay is prepared using a layered moist compaction method, the moisture content is controlled at 14.7% and the degree of compaction is about 85%. The clay is divided into five layers, each with a thickness of 50 mm. Before filling the next layer of soil, shaving the tamped soil surface is necessary to ensure a good contact. The gravel layer is compacted into three layers, the thickness of the lower two layers is 50 mm, and the thickness of the top layer is 30 mm.

After the sample preparation is completed, we conduct the saturation process. First, the sample is vacuumized with a vacuum pump. Then, we open the water inlet valve at the bottom of the sample to make the water in the water tank flow slowly into the sample. When the water surface reaches a predetermined height the water inlet valve is closed. After standing for a period of time, the cyclic loading is applied. In order to judge the water level inside the sample, a water-sensitive material is pasted on the inner wall of the sample cylinder, and the color of the water-sensitive material changes when it encounters water.

After the test, the gravel is removed, dried, and weighed. Next, the mud that adhered to gravel particles is cleaned, dried, and weighed again. The difference between the two weights corresponds to the weight of the mud (migrated fine particles).

3. Test results

3.1 Analysis of typical test curves

The curves of axial strain, excess pore water pressure, and dynamic stress within the soil during the M-6 test are shown in Fig. 4. The axial strain is the ratio of the axial displacement to the initial height of the sample.

As shown in Fig. 4(a), the axial strain of the sample increases rapidly within a few cycles number and then remains stable. After cyclic loading is applied, the gravel sinks into the subgrade soil and pushes the mud of the subgrade soil into the gravel void forming an interlayer, which is the primary reason for production of significant axial deformation within the samples. In addition, the compression of the gravel and the subgrade soil is another reason for the axial deformation of the samples.

The curves of axial strain and cycles number conform to the power function and can be calculated by the following empirical model.

$$\varepsilon_a = a(1-N^{-b}) \tag{3}$$

Where, ε_a is the axial strain of the sample, N is the cycles number, and a and b are the model parameters. Empirical model (3) was used to fit the axial strain of the samples in each test. The values of the model's parameters and correlation coefficient R^2 were obtained, as shown in Table 3. Moreover, we can see that parameter a is positively correlated with the dynamic stress amplitude and water level. Moreover, parameter b has no relation regarding the dynamic stress amplitude and water level. The correlation coefficients for these tests are all greater than 0.75, indicating that it is reasonable to use the empirical model (3) to fit the axial strain curves.

As seen from Fig. 4(b), at the initial stage of cyclic loading, a large excess pore water pressure is generated inside the sample. As the cyclic loading continues, the water inside the subgrade soil moves upward along the gravel, and the excess pore water pressure gradually decreases. Furthermore, as the depth of the subgrade soil increases, the excess pore water pressure for a given cycles number gradually increases. Fig. 4(c) shows the curves of excess pore water pressure and cycles number in a semi-logarithmic coordinate, we can see that the excess pore water pressure

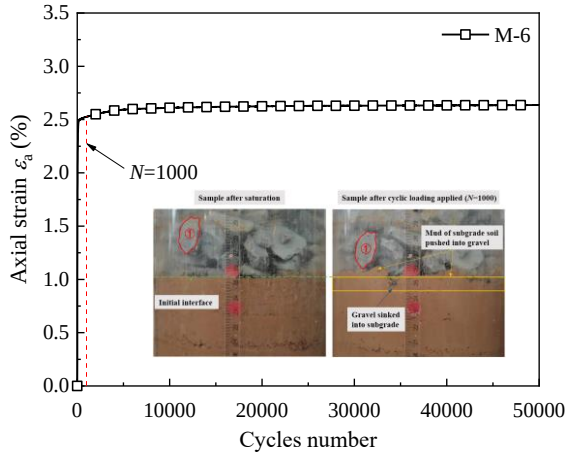

(a) Curves of axial strain and cycles number

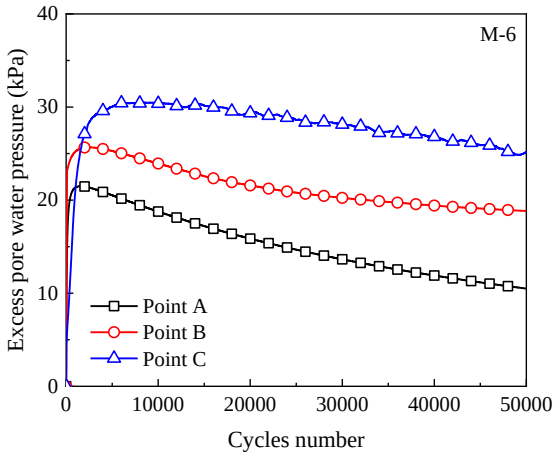

(b) Curves of excess pore water pressure and cycles number

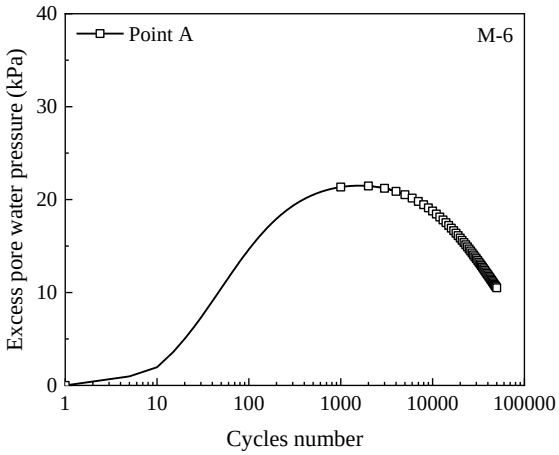

(c) Curves of excess pore water pressure and cycles number in a semi-logarithmic coordinate

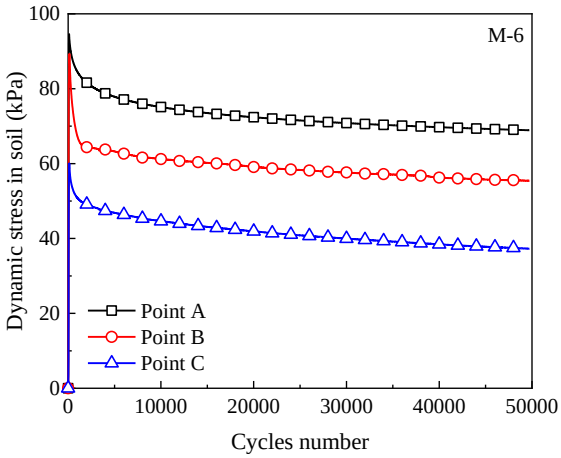

(d) Curves of dynamic stress within the soil and cycles number

Fig. 4 Typical test curves

increases rapidly at a decreasing rate as the cycles number increases up to 2000 cycles, after that it decreases gradually.

Fig. 4(d) shows that the dynamic stress within the soil first rapidly decreases and then slows with an increase in cycles number. As the depth of the subgrade soil increases, the dynamic stress within the soil gradually decreases, indicating that the influence of the external load gradually weakens with an increase in soil depth.

3.2 Influence of water level on the characteristics of subgrade mud pumping

3.2.1 Axial strain

Fig. 5 shows the influence of water level on the sample's axial strain during the mud pumping test. From Fig. 5 we can see that the axial strain of sample M-3 (the sample with a water level of +10 mm) first increases rapidly and then slowly with an increase in cycles number. The axial strain does not reach a stable value until the end of the test. For other samples when the water level is at or below the surface of the subgrade soil, the axial strain of the samples first increases rapidly and then stabilizes. As mentioned above, the axial deformation of samples M-6, M-7, M-8, and M-9 primarily comes from the generation of an interlayer, the compression deformation of the gravel layer and the subgrade soil. The axial deformation produced by both can be stabilized at the initial stage of the cyclic loading. In sample M-3, the axial deformation of the sample increases gradually with the dissipation of excess pore water pressure and the migration of the fine particles during later loading stages. In addition, we can also draw a conclusion that the axial strain decreases with decreasing water levels. For example, when the water level is +10 mm, the final axial strain of the sample is approximately 3.00%; when the water level drops to 0 mm, -10 mm, -50 mm and -150 mm, the final axial strain of the sample is 2.64%, 2.01%, 1.67%, and 0.31%, respectively.

3.2.2 Excess pore water pressure

Fig. 6 shows the curves of the excess pore water pressure and cycles number under different water levels. From Fig. 6, we see that during the tests M-3 (water level is +10 mm), M-6 (water level is 0 mm), and M-7 (water level is -10 mm), the excess pore water pressure at points A, B, and C all show the same trend of rapidly increasing followed by a slowly decrease. During the test M-8 (water level is -50 mm), the excess pore water pressure at points B and C increases rapidly to its peak value and then decreases slowly; however, at point A, the excess pore water pressure presents with

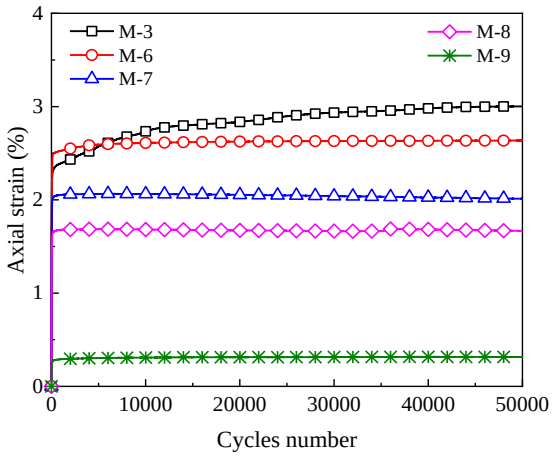

Fig. 5 Influence of water level on axial strain

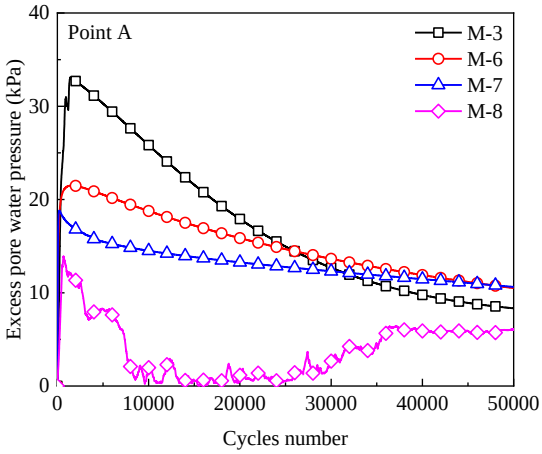

(a) Excess pore water pressure at point A

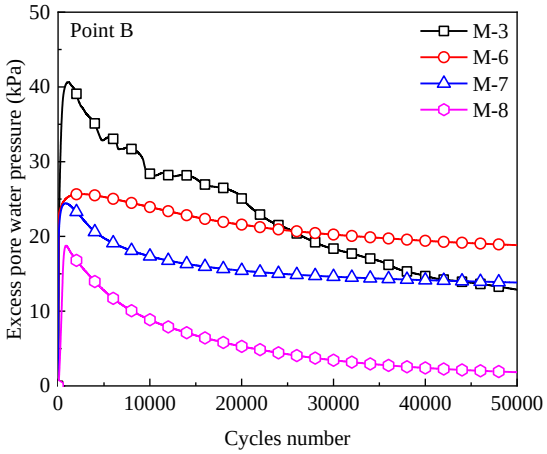

(b) Excess pore water pressure at point B

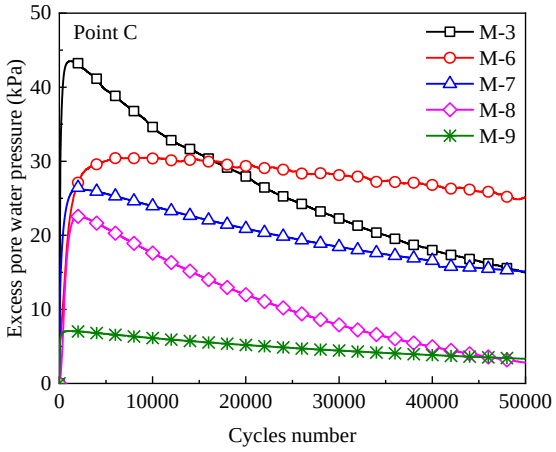

(c) Excess pore water pressure at point C

Fig. 6 Influence of water level on excess pore water pressure

irregular changes due to the soil being unsaturated. Furthermore, during the test M-9 (water level is -150 mm), the excess pore water pressure at point C first increases rapidly and then slowly dissipates under cyclic loading, and there is no excess pore water pressure at points A and B due to the soil being unsaturated. In general, the excess pore water pressure decreases significantly with a decrease in water level. For example, when the water level decreases from +10 mm to 0 mm, -10 mm, -50 mm, and -150 mm, the peak values of the excess pore water pressure at point C decrease from 43.52 kPa to 30.44 kPa, 26.44 kPa, 22.57 kPa, and 7.70 kPa, respectively.

3.2.3 Fine particles migration

We selected four reference points and recorded the fine particle migration height at a specific interval during the test.

Table 4 Weight of the migrated fine particles after the test

Test no.	Water levels / mm	Weight of migrated fine particles m/ (g)
M-1	+10	235.0
M-2	+10	433.0
M-3	+10	422.8
M-4	+10	365.0
M-5	+10	499.6
M-6	0	133.7
M-7	-10	79.0
M-8	-50	2.9
M-9	-150	3.6

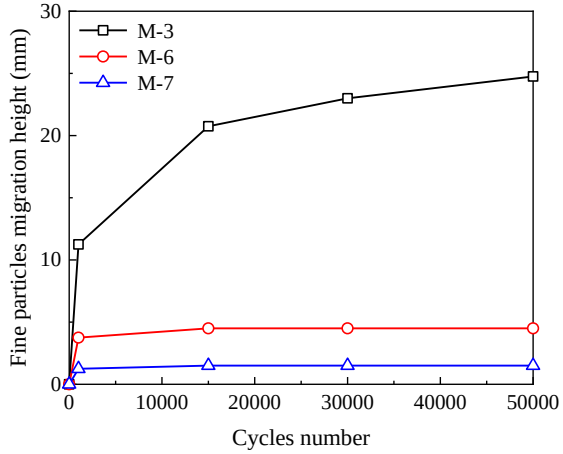

Fig. 7 Influence of water level on fine particle migration height

The average fine particle migration height at the four reference points was used for analysis. Fig. 7 shows the curves of fine particle migration height and cycles number under different water levels. Furthermore, only the curves of tests M-3 (water level is +10 mm), M-6 (water level is 0 mm), and M-7 (water level is -10 mm) are shown in Fig. 7. There is no fine particle migration occurred within tests M-8 (water level is -50 mm) and M-9 (water level is -150 mm). Fig. 7 shows that the fine particle migration height gradually increases with an increase in cycles number, and the increasing rate gradually decreases. Moreover, the migration of the fine particles primarily occurs at the initial stage of cyclic loading, because the sink gravel pushes the subgrade particles into its pores. Additionally, with a decrease in water level, the fine particle migration height decreases significantly.

Table 4 shows the weight of the migrated fine particles after the test. And we can see that the weight of the migrated fine particles decreases significantly with a decrease in water level. When the water level is no higher than -50 mm, the weight of the migrated fine particles is almost zero, indicating that a reduction in the subgrade water level can effectively mitigate the occurrence of subgrade mud pumping.

3.3 Influence of dynamic stress amplitude on the characteristics of subgrade mud pumping

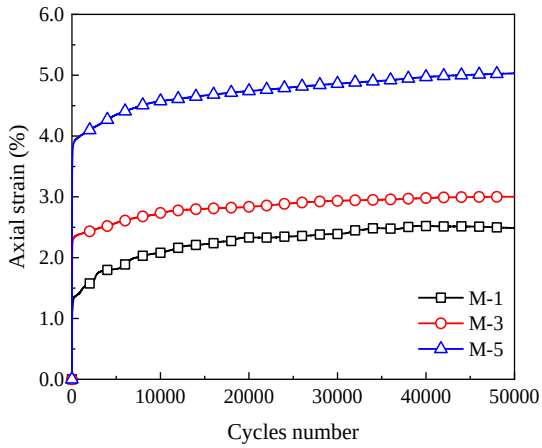

Fig. 8 Influence of dynamic stress amplitude on axial strain

Fig. 8 shows the influence of the dynamic stress amplitude on the curves of the axial strain and cycles number. It is revealed that the axial strain of the samples with a water level of +10 mm shows a nonlinear increase with an increase in cycles number; therefore, the rate of increase gradually decreases. Until the end of the test, the axial strain increases slowly. The increase in dynamic stress amplitude results in a larger axial deformation, due to the larger thickness of an interlayer.

Fig. 9 shows the influence of the dynamic stress amplitude on excess pore water pressure; therefore, we know that the excess pore water increases significantly with an increase in the dynamic stress amplitude. For example, when the dynamic stress amplitude increases from 50 kPa to 100 kPa and 200 kPa, the peak value of the excess pore water pressure increases from 25.08 kPa to 40.65 kPa and 70.03 kPa at point B, respectively.

Fig. 10 shows the influence of the dynamic stress amplitude on fine particle migration height. The weight of the migrated fine particles under different dynamic stress amplitudes is listed in Table 4. Both the fine particle migration height and the weight of the migrated fine particles increase under a greater dynamic stress amplitude meaning that an increase in the train axle load will lead to more severe subgrade mud pumping issues.

3.4 Influence of loading frequency on the characteristics of subgrade mud pumping

Figs. 11-13 shows the influence of loading frequency on the axial strain, excess pore water pressure, and fine particles migration height, respectively. We know that the loading frequency significantly affects axial strain, thus, the axial strain decreases with increasing frequency. For example, as the loading frequency increases from 1 Hz to 5 Hz to 10 Hz, the axial strain decreases from 3.60% to 3.00% to 2.46%, respectively. The excess pore water pressure is insensitive to the loading frequency. Furthermore, the fine particle migration height decreases slightly with an increase in loading frequency. When the loading frequency increases from 1 Hz to 5 Hz to 10 Hz, the particle migration height decreases from 24.8 mm to 24.75 mm to 21.25 mm, respectively.

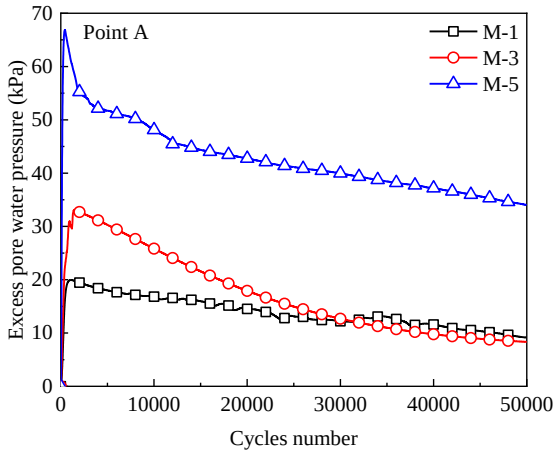

(a) Excess pore water pressure at point A

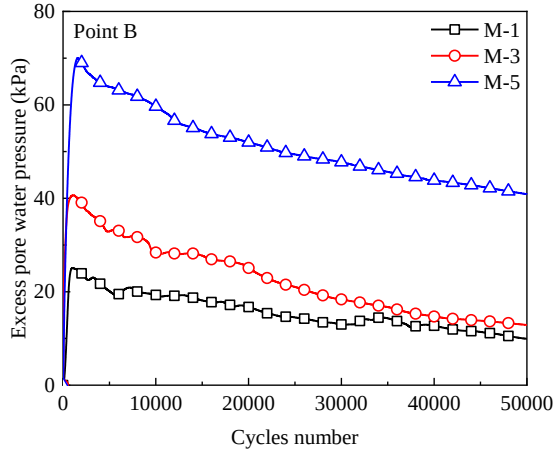

(b) Excess pore water pressure at point B

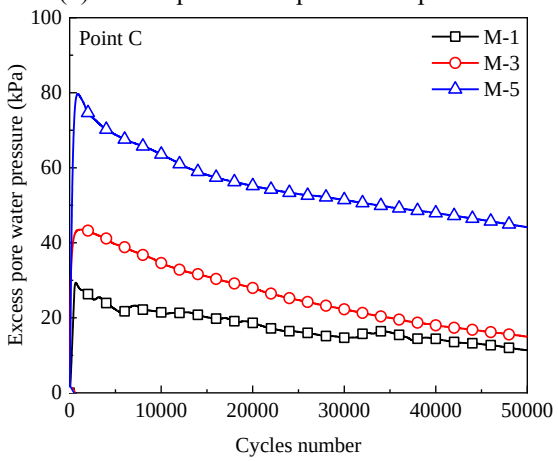

(c) Excess pore water pressure at point C

Fig. 9 Influence of the dynamic stress amplitude on excess pore water pressure

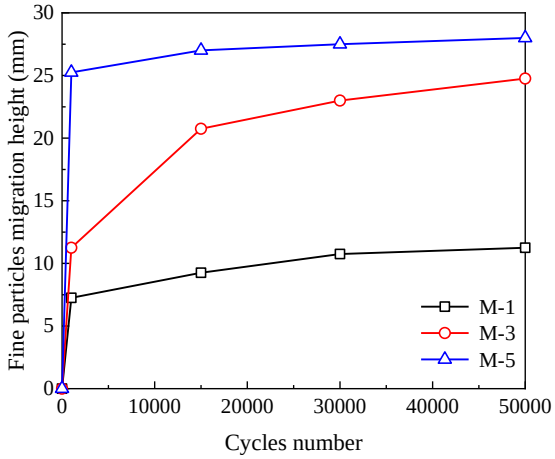

Fig. 10 Influence of dynamic stress amplitude on fine particles migration height

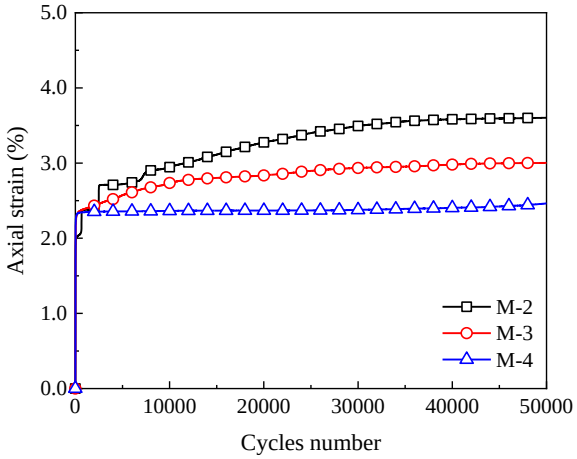

Fig. 11 Influence of loading frequency on axial strain

4. Conclusions

In this study, we conducted experiments that characterized the saturated clay subgrade and the influence of water levels on mud pumping. The characteristics of mud pumping are primarily reflected by the axial strain, excess pore water pressure, and fine particle migration; therefore, we obtain the following conclusions:

1) Under cyclic loading, the axial strain of the sample increases nonlinearly with an increase in cycles number; furthermore, the increasing rate of the axial strain decreases slowly. With an increase in cycles number, the excess pore water pressure first increases rapidly and then slowly decreases. The dynamic stress within the soil first decreases rapidly and then slowly. Based on test results, an empirical model for calculating the axial strain of the samples is presented.

2) With a decrease in water level, the axial strain decreases significantly. For example, when the water level height decreases from +10 mm to -150 mm, the axial strain decreases from 3.0% to 0.31%, respectively. The excess pore water pressure also decreases significantly with a decrease in water level, thus, causing a decrease of approximately 82% when the water level decreases from +10mm to -150 mm. The fine particle migration height and weight of the migrated fine particles all decrease significantly with a decrease in water level. And when the water level is -50 mm, the weight of the migrated fine particles is approximately 0.

3) An increase in the dynamic stress amplitude produces a significant axial strain and excess pore water pressure within the sample, therefore, aggravating the subgrade mud pumping issues. In general, the increase in loading frequency does not aggravate the degree of subgrade mud pumping, however it can significantly shorten the occurrence time.

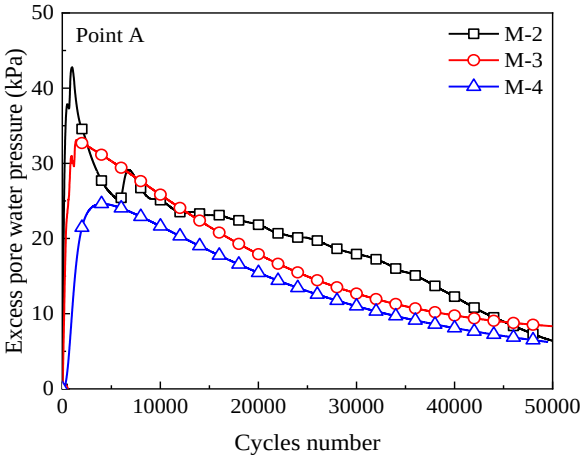

(a) Excess pore water pressure at point A

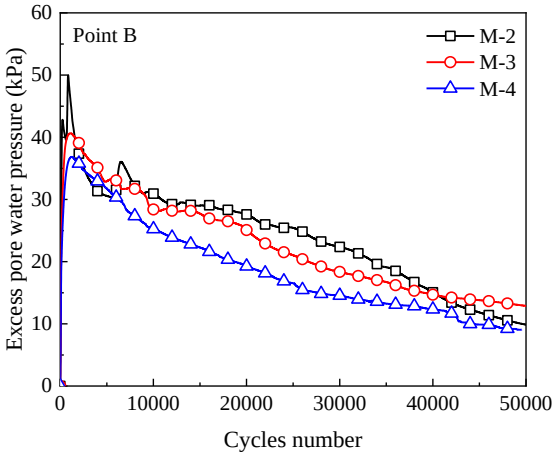

(b) Excess pore water pressure at point B

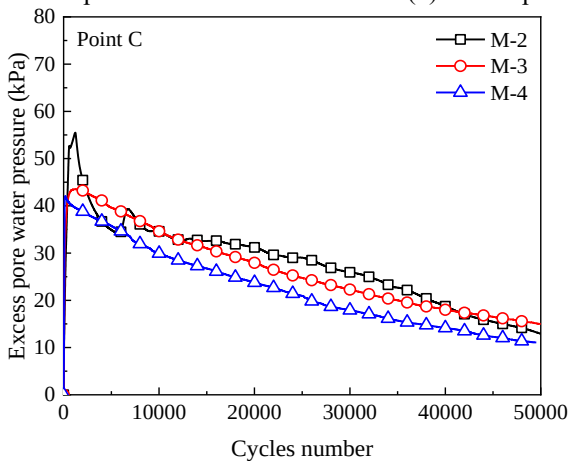

(c) Excess pore water pressure at point C

Fig. 12 Influence of loading frequency on excess pore water pressure

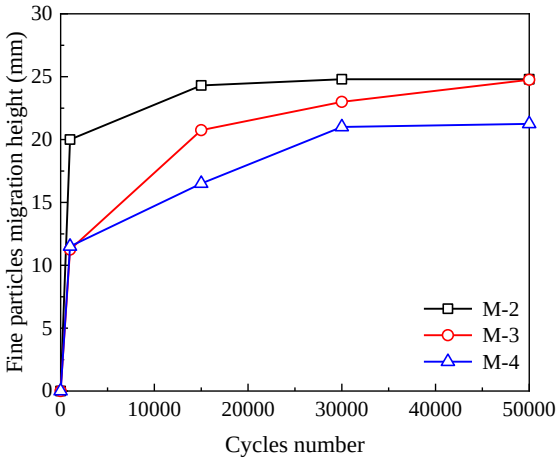

Fig. 13 Influence of loading frequency on fine particles migration height

4) It can be concluded that an appropriate reduction in water level can effectively mitigate the occurrence of subgrade mud pumping. In this study, when the water level is 50 mm lower than the subgrade soil surface, the issues of subgrade mud pumping no longer exist.

Acknowledgments

This study was supported by the National Natural Science Foundation of China (51978674). The laboratory tests were performed in the National Engineering Research Center of High-Speed Railway Construction Technology with significant support from Dr. Zhang of Central South University. The author is grateful to the anonymous reviewers for their constructive comments and suggestions. The authors thank AiMi Academic Services (www.aimieditor.com) for the English language editing and review services.

References

Bian, X.C., Jiang, J.Q., Jin, W.F., Sun, D.D., Li, W. and Li, X. (2016), "Cyclic and postcyclic triaxial testing of ballast and subballast", *J. Mater. Civil Eng.*, **28**(7), 04016032. http://doi.org/10.1061/(ASCE)MT.1943-5533.0001523.

Chen, B., Sun, D.A. and Jin, P. (2019), "Experimental study of the effect of microstructure on the permeability of saturated soft clays", *Geomech. Eng.*, **18**(1), 49-58. https://do.org/10.12989/gae.2019.18.1.049.

Ding, L., Zhang, J.H. and Deng, Z.H. (2021), "Effect of bound water on mechanical properties of typical subgrade soils in southern China", *Geomech. Eng.*, **5**(3), 263-281.

https://doi.org/10.12989/gae.2021.27.6.573.

Ding, Y., Jia, Y., Wang, X., *et al*. (2022), "Influence of particle size distribution and initial dry density on the characteristics of subgrade mud pumping", *Rock Soil Mech.*, **43**(9). http://doi.org/10.16285/j.rsm.2021.1971.

Duong, T.V., Cui, Y., Tang, A.M., Dupla, J.C., Canou, J., Calon, N. and Robinet, A. (2014), "Investigating the mud pumping and interlayer creation phenomena in railway sub-structure", *Eng. Geol.*, **171**, 45-58. http://doi.org/10.1016/j.enggeo.2013.12.016.

Hasnayn, M.M., McCarter, W.J., Woodward, P.K., Connolly, D.P. and Starrs, G. (2017), "Railway subgrade performance during flooding and the post-flooding (recovery) period", *T. Geotech.*, **11**, 57-68. http://doi.org/10.1016/j.trgeo.2017.02.002.

Hasnayn, M.M., McCarter, W.J., Woodward, P.K. and Connolly, D.P. (2020), "Railway subgrade performance after repeated flooding-large-scale laboratory testing", *T. Geotech.*, **23**, 100329. http://doi.org/10.1016/j.trgeo.2020.100329.

Hussaini, S.K.K., Indraratna, B. and Vinod, J.S. (2016), "A laboratory investigation to assess the functioning of railway ballast with and without geogrids", *T. Geotech.*, **6**, 45-54. http://doi.org/10.1016/j.trgeo.2016.02.001.

Indraratna, B. and Redana, I.W. (1998), "Laboratory determination of smear zone due to vertical drain installation", *J. Geotech. Geoenviron. Eng.*, **124**(2), 180-184. http://doi.org/10.1061/(ASCE)1090-0241(1998)124:2(180).

Indraratna, B., Attya, A. and Rujikiatkamjorn, C. (2009), "Experimental investigation on effectiveness of a vertical drain under cyclic loads", *J. Geotech. Geoenviron. Eng.*, **135**(6), 835-839. http://doi.org/10.1061/(ASCE)GT.1943-5606.0000006.

Indraratna, B., Ferreira, F.B., Qi, Y.J. and Ngoc Ngo, T. (2018), "Application of geoinclusions for sustainable rail infrastructure under increased axle loads and higher speeds", *Innov. Infrastruct. Solutions*, **3**(1), 1-21. http://doi.org/10.1007/s41062-018-0174-z.

Indraratna, B., Ngo, N.T. and Rujikiatkamjorn, C. (2011), "Behavior of geogrid-reinforced ballast under various levels of fouling", *Geotext. Geomembranes*, **29**(3), 313-322. http://doi.org/10.1016/j.geotexmem.2011.01.015.

Indraratna, B., Rujikiatkamjorn, C., Ewers, B. and Adams, M. (2010), "Class A prediction of the behavior of soft estuarine soil foundation stabilized by short vertical drains beneath a rail track", *J. Geotech. Geoenviron. Eng.*, **136**(5), 686-696. http://doi.org/10.1061/(ASCE)GT.1943-5606.0000270.

Indraratna, B., Singh, M. and Nguyen, T.T. (2020a), "The mechanism and effects of subgrade fluidisation under ballasted railway tracks", *Railway Eng. Sci.*, **28**(2), 113-128. http://doi.org/10.1007/s40534-020-00210-1.

Indraratna, B., Singh, M., Nguyen, T.T., Leroueil, S., Abeywickrama, A. and Kelly, B. (2020b), "Laboratory study on subgrade fluidization under undrained cyclic triaxial loading", *Can. Geotech. J.*, **57**(11), 1767-1779. http://doi.org/10.1139/cgj-2019-0350.

Indraratna, B., Sun, Q., Ngo, N.T. and Rujikiatkamjorn, C. (2017), "Current research into ballasted rail tracks: model tests and their practical implications", *Aust. J. Struct. Eng.*, **18**(3), 204-220. http://doi.org/10.1080/13287982.2017.1359398.

Ito, T. (1984), "Actual situation of mud pumping and its countermeasures", *Quarterly Reports of the Railway Technical Research Institute*.

Kashani, H.F., Hyslip, J.P. and Ho, C.L. (2017), "Laboratory evaluation of railroad ballast behavior under heavy axle load and high traffic conditions", *T. Geotech.*, **11**, 69-81. http://doi.org/10.1016/j.trgeo.2017.04.002.

Leng, W.M., Mei, H.H., Nie, R.S., Zhao, C., Liu, W. and Su, Y. (2018a), "Full-scale model test of heavy haul railway subgrade", *J. Vib. Shock*, **37**(4), 1-6. http://doi.org/10.13465/j.cnki.jvs.2018.4.001.

Leng, W.M., Su, Y., Teng, J.D., *et al.* (2018b), "Analysis and evaluation on physical characteristics of fine-grained soils prone to mud pumping", *J. China Railway Soc.*, **40**(1), 116-122. http://doi.org/10.3969/j.issn.1001-8360.2018.01.018.

Li, P.F., Liu, H.C., Zhao, Y. and Li, Z. (2018), "A bottom-to-up drainage and water pressure reduction system for railway tunnels", *Tunn. Undergr. Sp. Tech.*, **81**, 296-305. http://doi.org/10.1016/j.tust.2018.07.027.

Liu, D., Fu, H.L., Zhu, X.Z., Liu, Y.S. and Rao, J.Y. (2013), "Study on the remediation of mud-pumping", *Appl. Mech. Mater.*, **275-277**, 1560-1563. http://doi.org/10.4028/www.scientific.net/AMM.275-277.1560.

Nagrale P.P. and Patil A.P. (2017), "Improvement in engineering properties of subgrade soil due to stabilization and its effect on pavement response", *Geomech. Eng.*, **12**(2), 257-267. https://doi.org/10.12989/gae.2017.12.2.257.

Nguyen, T.T., Indraratna, B., Kelly, R., Phan, N.M. and Haryono, F. (2019), "Mud pumping under railtracks: mechanisms, assessments and solutions", *Aus. Geomech. J.*, **54**(4), 59-80.

Nie, R.S., Leng, W.M., Su, Y., *et al.* (2018), "Physical and mechanical properties of mud pumping soils in railway subgrade bed", *J. Southwest Jiaotong Univ.*, **53**(2), 286-295. http://doi.org/10.3969/j.issn.0258-2724.2018.02.010.

Qiao, L.J. (2006), "Treatment of subgrade mud pumping in K245 ~ K462 of Jingtong Line", *Railway Eng.*, **10**, 75-76. http://doi.org/10.3969/j.issn.1003-1995.2006.10.029.

Saride, S., Pradhan, S., Sitharam, T.G., *et al*. (2013), "Numerical analysis of geocell reinforced ballast overlying soft clay subgrade", *Geomech. Eng.*, **5**(3), 263-281. http://doi.org/10.12989/gae.2013.5.3.263.

Singh, M., Indraratna, B. and Rujikiatkamjorn, C. (2019), "Use of geosynthetics in mitigating the effects of mud pumping: a railway perspective", *Geotech. T. Infrastruct.*, **29**, 609-618. https://doi.org/10.1007/978-981-13-6713-7_48.

Sun, Q.D., Indraratna, B. and Nimbalkar, S. (2016), "Deformation and degradation mechanisms of railway ballast under high frequency cyclic loading", *J. Geotech. Geoenviron. Eng.*, **142**(1), 04015056. http://doi.org/10.1061/(ASCE)GT.1943-5606.0001375.

Tang, L.S., Chen, H.K., Sun, Y.L., *et al.* (2018), "Traffic-load-induced dynamic stress accumulation in subgrade and subsoil using small scale model tests", *Geomech. Eng.*, **16**(2), 113-124. http://doi.org/10.12989/gae.2018.16.2.113.

Trani, L.D.O. and Indraratna, B. (2010a), "Assessment of subballast filtration under cyclic loading", *J. Geotech. Geoenviron. Eng.*, **136**(11), 1519-1528. http://doi.org/10.1061/(ASCE)GT.1943-5606.0000384.

Trani, L.D.O. and Indraratna, B. (2010b), "Experimental investigations into subballast filtration behaviour under cyclic conditions", *Aust. Geomech. J.*, **45**(3), 123-1333.

Yang, Q.Y. and Zha, K. (2006), "Using horizontal water collecting pipes to remedy mud pumping", *Subgrade Eng.*, **2**, 130-132. http://doi.org/10.3969/j.issn.1003-8825.2006.02.053.

Yang, Z.H., Yue, Z.R. and Tai, B.W. (2021), "Investigation of the deformation and strength properties of fouled graded macadam materials in heavy-haul railway subgrade beds", *Constr. Build. Mater.*, **273**, 121778. http://doi.org/10.1016/j.conbuildmat.2020.121778.

Yu, H.B. (2013), "Study on the treatment scheme for diseases in tunnel base by well point dewatering under the condition of heavy axle load train on existing railway", *China Railway Sci.*, **34**(4), 54-59. http://doi.org/10.3969/j.issn.1001-4632.2013.04.09.

GC